Solar RRL
www.solar-rrl.com

Mixed Dimensional Perovskites Heterostructure for Highly Efficient and Stable Perovskite Solar Cells

Chuangye Ge, Jian-Fang Lu, Mriganka Singh, Annie Ng, Wei Yu, Haoran Lin, Soumitra Satapathi, and Hanlin Hu**

Heterojunctions constructed upon multidimensional perovskites (1D/3D or 2D/3D) has emerged as an effective approach to improve the photovoltaic performance and stability of perovskite solar cells (PSCs). Herein, 1D trimethyl sulfonium lead triiodide (Me_3SPbI_3) 1D Me_3SPbI_3 nanoarrays are successfully synthesized via a two-step method in aqueous condition, which reflects excellent water resistivity and environmental stability. By incorporating this 1D Me_3SPbI_3 into lead halide 3D perovskites, heterostructural 1D/3D perovskite photoactive layer with improved morphology, crystallinity, enhanced photoluminescence lifetime, and reduced carrier recombination in comparison to its 3D counterpart is obtained. Moreover, an efficient and stable 1D/3D PSCs with power conversion efficiency (PCE) of 22.06% by using this 1D/3D perovskite are demonstrated. It noticeably maintained 97% of their initial efficiency after 1000 h storage under ambient condition (RH≈50%) without encapsulation. Our study opens up the design protocol for the development of next-generation highly efficient and stable perovskite solar cells.

1. Introduction

Organic–inorganic hybrid perovskite solar cells (PSCs) have attracted tremendous attention due to their unique optoelectronic properties, power conversion efficiency (PCE), cost-effectiveness, and solution processability.[1–5] Within a few years, the PCE of 3D (3D) perovskite materials based PSCs has rapidly soared from 3.8% to 25.8%, which is comparable with that of the state-of-art monocrystalline silicon solar cells.[6–8] However, because of their intrinsic structural characteristics, 3D perovskites still suffer from poor stability in ambient conditions, when exposed to UV light, moisture, heat, and electric field, which limits the commercialization potential of the PSCs.[9–13] To address the long-term stability issue, 1D perovskites are emerging as ideal alternatives due to their structural diversity, tunable optical properties, and superior environmental stability.[14–16] From the molecular level, the 1D perovskites, are different from the morphological 1D nanowires, nanofibers, and nanorods.[17] Typically, the $[PbX_6]^{4-}$ octahedral surrounded by organic cations are corner-sharing, edge-sharing, or face-sharing to form a 1D perovskites chain.[18,19] 1D perovskite show superb stability by taking the advantage of the improvement of the skeleton strength attribute to the "shoulder to shoulder" arrangement of $[PbX_6]^{4-}$and the protection of organic cations.[20] By incorporating large organic cations into the 3D perovskite precursor or post-

C. Ge, M. Singh, H. Lin, H. Hu
Hoffmann Institute of Advanced Materials
Postdoctoral Innovation Practice Base
Shenzhen Polytechnic
Nanshan District, Shenzhen 518055, P. R. China
E-mail: hanlinhu@szpt.edu.cn

J.-F. Lu
School of Chemistry and Chemical Engineering
Guangxi University for Nationalities
Nanning, Guangxi 530006, P. R. China

M. Singh
Research Center for Applied Sciences
Academia Sinica
Taipei 11529, Taiwan

The ORCID identification number(s) for the author(s) of this article can be found under https://doi.org/10.1002/solr.202100879.

DOI: 10.1002/solr.202100879

A. Ng
Department of Electrical and Computer Engineering
School of Engineering and Digital Science
Nazarbayev University
Kabanbay Batyr Ave. 53, Nur-Sultan 010000, Kazakhstan

W. Yu
State Key Laboratory of Catalysis
Dalian Institute of Chemical Physics
Chinese Academy of Sciences
Dalian National Laboratory for Clean Energy
Dalian, Liaoning 116023, P. R. China

S. Satapathi
Department of Physics
Indian Institute of Technology
Roorkee, Uttarakhand 247667, India
E-mail: soumitra.satapathi@ph.iitr.ac.in

processing a thin layer of large cation on top of the 3D perovskite film, a mixed or layered multidimensional PSCs could be fabricated which are stable and possess has both the environmentally stable features and promising photovoltaic performance.[21–25] However, only a handful of organic cation crystalize into 1D perovskite structure. Bi et al. employed an aliphatic fluorinated additive 1,1,1-trifluoro-ethyl ammonium iodide (FEAI) in methylammonium lead iodide ($MAPbI_3$) perovskite to improve the environmental stability and PCE of the PSCs.[26] Fan et al. introduced 2-(1H-pyrazol-1-yl) pyridine (PZPY) into 3D perovskite which can not only produce a series of 1D or 1D D^{-1} heterojunctions, but also obtain a thermodynamic self-healing ability, and improve the long-term stability.[27] Liu et al. constructed a lattice-matched structure by incorporating 1D PbI_2-bipydine (BPy) perovskite into 3D perovskite to slow down ion migration with enhanced stability of perovskite film and device.[20] Yu et al. demonstrated that the introduction of hydrazinium (HA) into formamidinium lead iodide ($FAPbI_3$) perovskite can stabilize the α-phase $FAPbI_3$ by forming 1D/3D hybrid perovskite structure.[28] In the work of Gao et al., thiazole ammonium iodide (TAI) was applied to form a 1D passivation layer of $TAPbI_3$ on the 3D perovskite film and the corresponding device displayed higher PCE and better long-term operational stability as compared to the reference device.[29] Similarly, Xu et al. employed a 1D $PyPbI_3$ (Py: pyrrolidine) perovskitoid layer on the 3D $FAPbI_3$-based perovskite to stabilize the black perovskite phase and enhance the performance of the achieved device.[30] Chen's group introduced a thin layer of 1D/3D heterostructure by in situ cross-linking of polymerizable propargylammonium (PA^+) to facilitate the interfacial charge transport and release the residual tensile strain in the perovskite films.[31] Very recently, Bi et al. employed 2-diethylaminoethylchloride hydrochloride (DEAECCl) to prepare a novel 1D perovskitoid, which can induce the growth of 1D@3D perovskite structure, leading to better crystallinity and charge transport, and reduced remnant tensile strain in 3D perovskite film, thereby enhance the PCE and stability of the devices.[9] However, steric hindrance induced by large organic cation in 1D perovskite leads to poor and anisotropic charge conductivity resulting lower PCE value. Thus, further research is needed to explore new organic cation leading to 1D perovskite structure which can be synchronized with 3D perovskite.

Typically, the conventional ammonium based organic cations are easily decomposed due to the presence of N—H bonds, which can be further hydrolyzed by water molecules in the air. To address this stability issue, sulfonium-containing cations, such as including trimethylsulfonium (Me_3S^+), trimethylsulfoxonium (Me_3S^+), and butyldimethylsulfonium ($BDMS^+$), have been investigated and these cations display great potential for constructing stable perovskite materials and related optoelectronic devices.[32] Among them, it has been demonstrated that Me_3SI, a novel sulfur-based cation, could react with metal halide and form stable 1D perovskites Me_3SBX_3 in or $(Me_3S)_2BX_3$. Kaltzoglou and co-workers developed Me_3SPbI_3 and investigated its structural and optoelectronic properties, which showed high stability under moist air conditions and up to 200 °C for the first time.[33,34] Additionally, they also reported the crystal structure and physical properties of $(Me_3S)_2SnX_6$ (X = Cl, Br, I) compounds as well as the application of $((CH_3)_3S)_2SnI_6$ in dye-sensitized solar cells with enhanced performance and stability.[21,35,36] Afterward, Hu et al. prepared 1D Me_3SPbI_3 nanorod arrays and employed it for solar cells and photodetectors, which exhibited excellent stability over two months under ambient conditions.[37] Inspired by this, we have synthesized Me_3SPbI_3 nanoarray and fabricated PSCs device based on this nanoarray shows, PCE over 2% and good long-term stability, which is higher than the previously reported 1D perovskites based devices. Interestingly, after incorporating into 3D perovskites, the heterostructure 1D/3D perovskites exhibits prolonged photoluminescence lifetime and reduced charge recombination compared with its 3D counterpart. Finally, an efficient and stable 1D/3D device is realized, exhibiting a PCE of 22.06%, and maintaining 97% of their initial efficiency after 1000 h storage in moisture, illumination, and heat.

2. Results and Discussion

In this work, we successfully synthesized Me_3SPbI_3 nanoarrays film via a two-step aqueous phase approach for the first time, where the PbI_2 solution was spin-coated on the ITO substrates and then the substrates were immersed into the Me_3SI aqueous solution (1 mg mL^{-1} in DI water) for various time at 60 °C, achieving different nanostructured Me_3SPbI_3 nanoarrays. These films were characterized by XRD and SEM to study the reaction mechanism between Me_3SI and PbI_2. From the SEM image in **Figure 1**a, a layered PbI_2 film with some nano-sized holes are deposited on the ITO, well agreed with the previous reports.[37,38] After immersing for 1 min, an uniform Me_3SPbI_3 nanoarray is produced by the reaction of Me_3SI and PbI_2, which can be clearly observed from Figure 1b. When we prolonged the dipping time over 1 h, it randomly distributed some large-size nanoparticles or hexagonal nanorods with length of several micrometres (Figure 1c,d). All these results indicate a good chemical stability of the Me_3SPbI_3 against water molecules. Figure 1e shows the XRD patterns of the Me_3SPbI_3 nanoarrays films with various soaking time in aqueous solution with continuous heating at 60 °C. For the pure PbI_2, only one main characteristic peak located at 12.6° corresponding to (001) plane.[30] After increasing of the dipping time, the peak of PbI_2 gradually weakened while some new peaks were observed at 10.6°, 24.2°, and 31.2°, corresponding to the (100), (201), and (202) reflections of 1D Me_3SPbI_3, indicating the successful formation of hexagonal Me_3SPbI_3. The UV absorption and the steady-state PL spectrum are shown in Figure S1, Supporting Information, the absorption peak ranges from 350 to 700 nm while a broad emission peak of Me_3SPbI_3 nanorod arrays is observed at about 520 nm perovskite with good crystallinity and purity.[30,32] Meanwhile, we also measured XRD for the sampled prepared at 25 °C. However, we found that there was still a residual peak for PbI_2 after even 12 h dipping, suggesting a slow formation of Me_3SPbI_3 nanoarrays as shown in Figure S2, Supporting Information. In order to study the crystal phase of Me_3SPbI_3, we prepared a needle-like 1D perovskite single crystal (SCs) by following the antisolvent method as reported in our previous work.[37] The well-defined diffraction peaks (Figure 1f) suggested a good crystallinity of the obtained Me_3SPbI_3 nanoarrays, which can be indexed as the hexagonal crystal structure with space group of $P6_{3mc}$ (No.186) and lattice constants a = b = 9.615 Å, c = 7.950 Å, a = b = 90°, c = 120°. As shown in Figure 1g,h,

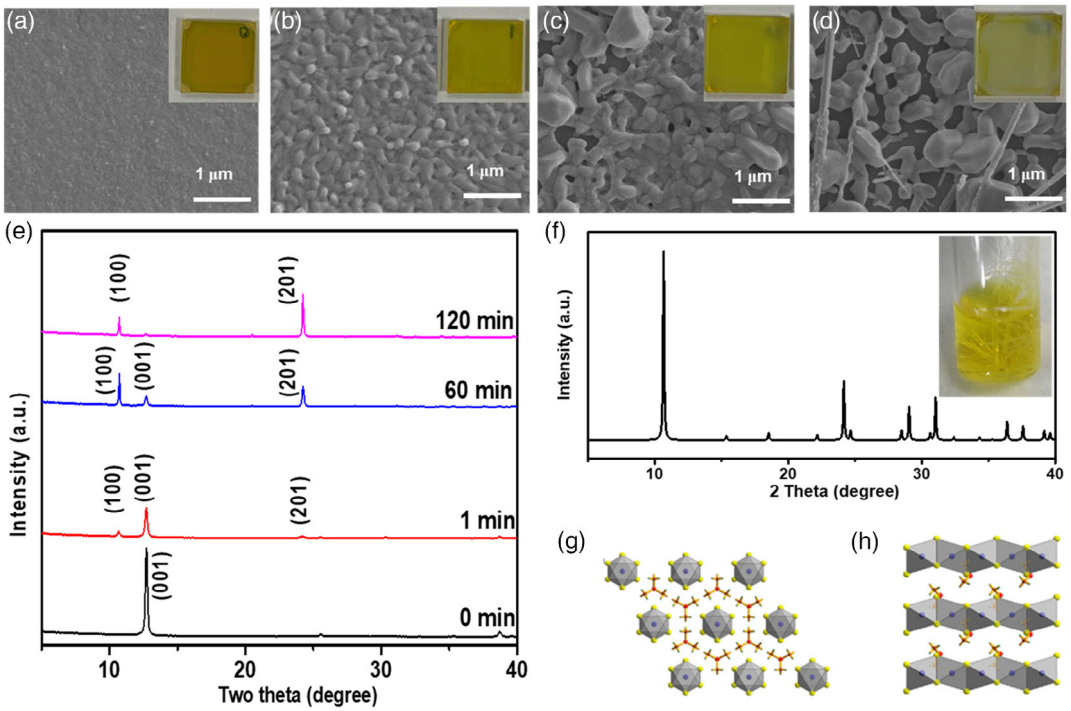

Figure 1. a–e) SEM images and XRD patterns of PbI_2 and 1D Me_3SPbI_3 nanoarrays obtained by dipping in Me_3SI solution for different time from 0 to 120 min. Photograph of as prepared 1D perovskite of Me_3SPbI_3. f) XRD of Me_3SPbI_3 single crystal. g–h) Crystal structure of Me_3SPbI_3 from different faces of $2 \times 2 \times 2$ unit cell generated by the Diamond software with the CCDC file of 1 547 868. (g) (010) view and (h) (100) view. (d) Inset of the SEM images are the corresponding optical photographs and e-h) the inset of XRD is the photograph of as prepared 1D single crystal of Me_3SPbI_3.

the face-shared $[PbI_6]^{4-}$ octahedral form 1D chains along the c axis while the Me_3S^+ cations occupy the interstitial sites between $[PbI_6]^{4-}$ in the 1D chains, which are similar to the yellow and thermo-dynamically stable δ-$FAPbI_3$ phase.[39]

What is more, we also prepared the 1D perovskite thin film in the organic solution (IPA) of Me_3SI, and a uniform and well-crystallized Me_3SPbI_3 nanoarray (**Figure 2**a) was deposited on the ITO substrate, displaying a good out-of-plane orientation with length around 2–3 μm as shown in Figure 2b. We fabricated a planar-type PSC with the structure of ITO/SnO_2/Me_3SPbI_3/spiro-OMeTAD/Au with the as prepared 1D Me_3SPbI_3 nanoarrays as absorber. Figure 2c displays the *J–V* curves with different scan directions, showing a V_{oc}, J_{sc}, FF, and PCE of 0.99 V, 3.76 mA cm^{-2}, 0.56, and 2.09%, respectively, without hysteresis, which is higher than some previous reports using pure 1D perovskite materials as the sensitizers as summarized in Table S1, Supporting Information.[9] However, low efficiency of Me_3SPbI_3 based solar cell could be attributed to the rough and porous nature of the perovskite film and the relatively narrow absorption range up to around 530 nm compared with other typical 3D perovskite such as $MAPbI_3$ or $FAPbI_3$.[32,37] It was a challenge for the preparation of an uniform and homogeneous film due to the large tolerance factor in1D crystal structures[34,37] obtained via two-step solution process. Due to the poor solubility of Me_3SI in the common solvents, such as DMF, DMSO, or γ-butyrolactone, the surface coverage of perovskite film is poor which results in lower PCE through one-step solution process method. Meanwhile, according to the theoretical calculation the Shockley–Queisser limit, for single-junction Me_3SPbI_3-based PSCs, it is possible to achieve a V_{oc}, J_{sc}, and FF of 1.96 V, 8.96 mA cm^{-2} of and 93.15%, respectively, with a PCE of 16.37%.[40] Therefore, there is a room for improvement of the performance of Me_3SPbI_3-based PSCs. The corresponding EQE and integrated J_{sc} (3.76 mA cm^{-2}) are exhibited in Figure 2d. The device also shows excellent long–term stability with negligible decrease of photovoltaic performance after 500 h storage in ambient condition with 50% RH as shown in Figure 2e. Furthermore, the XRD results of Figure 2f confirms that the nanoarrays films show good stability over 50 days under the same storage condition.

The surface morphology of the 3D and 1D/3D perovskite was characterizing via scanning electron microscope (SEM), as shown in **Figure 3**a–d. It can be revealed that the grain size of 1D/3D perovskite tends to be smaller than the reference 3D sample, which is consistent with previously published data.[27,30] Generally, the metal halide bonds of $[PbI_6]^{4-}$ octahedrons in 3D perovskites could easily break down and produce lower dimensional confined materials including 0D quantum, 1D linear arrangement, or 2D layered structure through structural reorganization.[41,42] The crystal lattice at the junction domains are possibly distorted and/or rearranged, resulting in the reduction of the grain size.[43] In Figure 3c, 1D nanorods are observed with vertical orientation and the diameters are several hundreds of nanometers. The length of this nanorods increased with increasing the addition of Me_3SI (Figure 3d). In Figure S3, Supporting Information, we can clearly see that the 1D nanorods distribute

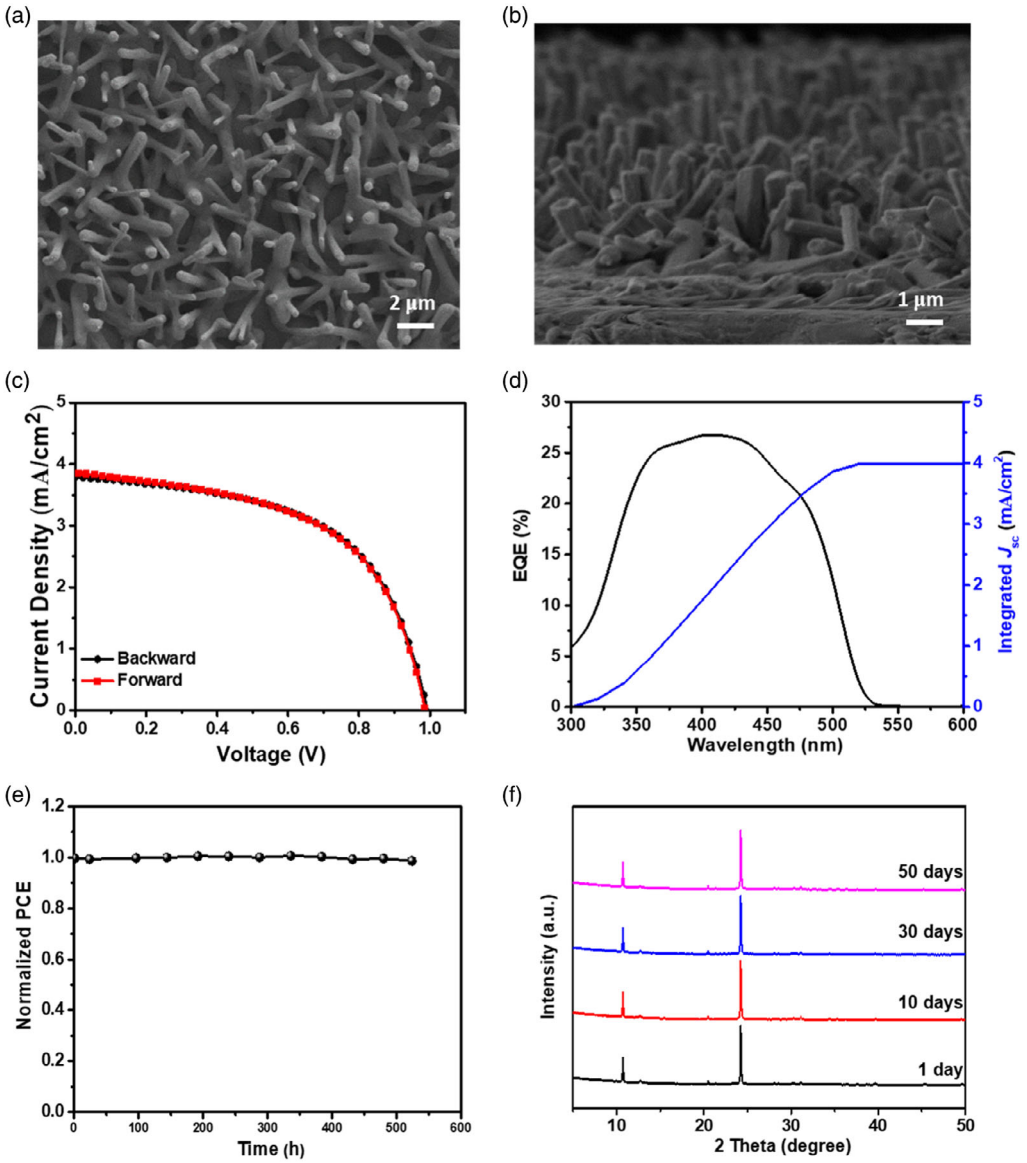

Figure 2. a) SEM image top views and b) cross-sectional SEM image of the as-prepared 1D perovskite of Me_3SPbI_3 c) *J–V* curves of the 1D perovskite of Me_3SPbI_3-based device with different scan directions. d) The corresponding EQE and integrated J_{sc} and e) long-term stability for Me_3SPbI_3-based device. f) XRD patterns of the prepared Me_3SPbI_3 film after storage in ambient condition with over 50% RH for different time.

randomly on the surface. Unlike the top-view SEM image, no clear 1D nanorod crystals can be noticed, which might be due to limited growth since the steric hindrance among the 3D perovskite grains. To study the moisture stability of the 3D and 1D/3D perovskite film, we also measure the contact angle as shown in the inset of each SEM image. The results are 63.27°, 80.15°, 90.83°, and 103.70°, indicating a better aprotic property, which attributes to the hydrophobic nature of Me_3SI and also confirm that the 1D/3D perovskite films have better resistance to moisture.[21,44] We compared the XRD patterns of 3D perovskite and 1D/3D perovskite in Figure 3e. It can be clearly seen that the 3D perovskite shows a small characteristic peak of PbI_2 (001) at around 12.6° and three peaks at 14.1°, 24.4°, and 28.2°, corresponding to the (110), (111), and (002) plane of 3D perovskite films. After the introduction of Me_3SI, this small peak disappeared and another new peak at 10.7° is observed with gradually increasing amount of Me_3SI, which is obviously different from the XRD of 3D perovskite films and can be deduced to the (100) plane of 1D Me_3SPbI_3, indicating the formation of 1D/3D perovskite. The UV–vis absorption and the corresponding PL spectrum for the 3D and 1D/3D perovskite films are displayed in Figure 3f,g. With the addition of a small amount of Me_3SI, a minor blue-shift in comparison to that of the 3D film is observed, which may be attributed to the stronger quantum confinement in the presence of the 1D Me_3SPbI_3.[45] Compared to the 3D film, the 1D/3D films exhibit more uniform distribution and a higher PL intensity, which can be attributed to better charge extraction/transport, suppressed crystal defects, and reduced nonradiative

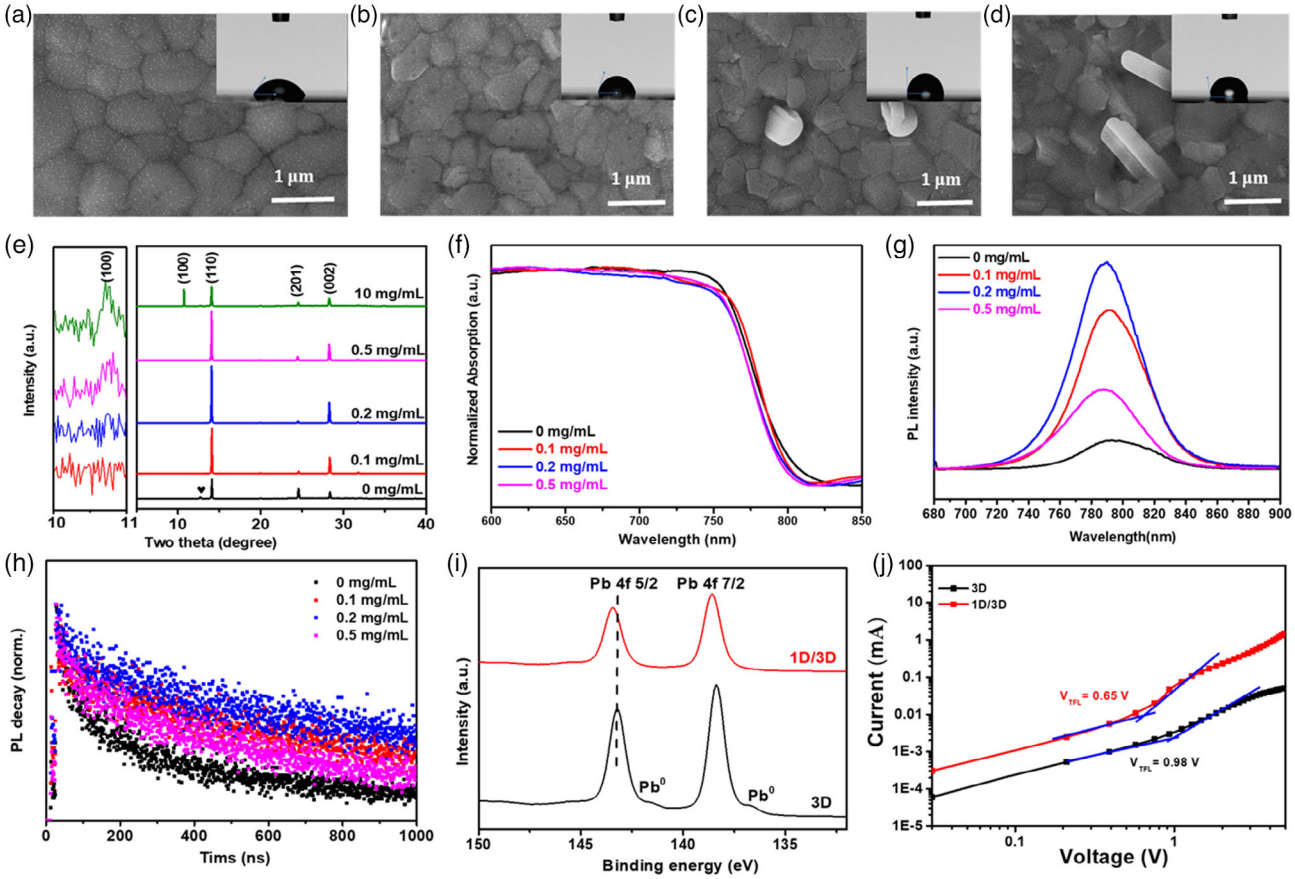

Figure 3. a–d) SEM images, e) XRD patterns, f) UV–vis absorption, g) steady-state photoluminescence, and h) time-resolved photoluminescence spectra of the 1D/3D perovskite films. i) XPS of Pb 4f core-level spectra for perovskite films. j) Dark *J–V* curves of electron-only devices with the structure of glass/ITO/SnO_2/perovskite/PCBM/Au. Inset of the SEM images are the corresponding water contact angle test results.

recombination.[46–48] Besides, the emission peak for 1D/3D films shifted gradually from 793 nm (control) to 790 nm (0.2 mg mL^{-1}), which can be deduced to a reduced trap density of the 1D/3D films. In order to confirm PL observation, the time-resolved photoluminescence (TRPL) measurements were carried out on glass/perovskite samples with and without 1D Me_3SPbI_3. The wavelength of excitation light was 440 nm and the PL decay is shown in Figure 3h. The lifetime is extracted by fitting the PL decay with a biexponential function, and summarized in Table S2, Supporting Information. Here, τ_1 represents the charge transfer dynamics at the interface, and τ_2 is related to nonradiative recombination of photogenerated carriers.[49] The average decay lifetime increased from 319.80 to 650.70 ns for 3D and 1D/3D perovskite films, respectively, suggesting a reduced nonradiative recombination loss in 1D/3D films.[50] Our TRPL study confirmed defect passivation in 1D/3D perovskite films. X-ray photoelectron spectroscopy (XPS) measurement was carried out to further study the effect of the introduction of 1D perovskite. As shown in Figure 3i, two peaks of Pb^{2+} $4f_{7/2}$ and Pb^{2+} $4f_{5/2}$ at 138.4 and 143.2 eV are present in the 3D film, respectively. However, for 1D/3D perovskite films, they are shifted to 138.6 and 143.4 eV, respectively, could be ascribed to the strong electronic interactions between Me_3SI and Pb^{2+} due to the formation of Pb—S bond.[51,52] In addition, two small peaks are also observed at 136.6 and 141.5 eV assigned to the Pb^0 $4f_{7/2}$ and Pb^0 $4f_{5/2}$ for 3D perovskite films, which are suppressed in 1D/3D perovskite films. It has been accepted widely that the metallic lead clusters (Pb^0) can form deep defects and trap the free carriers in perovskite films, leading to a severe nonradiative recombination and a deteriorate of device performance and long term stability.[53,54] Thus, the reduced Pb^0 defect caused by the passivation of 1D Me_3SPbI_3 are beneficial for the device performance and stability. Besides, in contrast to the pure 3D perovskite film, the lower dimension counterpart owns higher bandgap, leading to a strong suppression of nonradiative at the boundaries.[29] Moreover, trap-state density of the perovskite film was investigated by the space-charge-limited-current (SCLC) method. Figure 3j shows the dark *J–V* characteristics of the electron-only devices fabricated with the structure of glass/ITO/SnO_2/PCBM/Au. The trap-state density was calculated by the trap-filled limit voltage using the equation: $N_t = 2\varepsilon_0\varepsilon_r V_{TFL}/(qL^2)$, where ε_0 is the vacuum permittivity, ε_r is the relative dielectric constant ($\varepsilon_r = 46.9$), V_{TFL} is the onset voltage of the trap-filled limit region, q is the elementary charge, and $_L$ is the thickness of perovskite film.[55] The trap state densities are estimated to

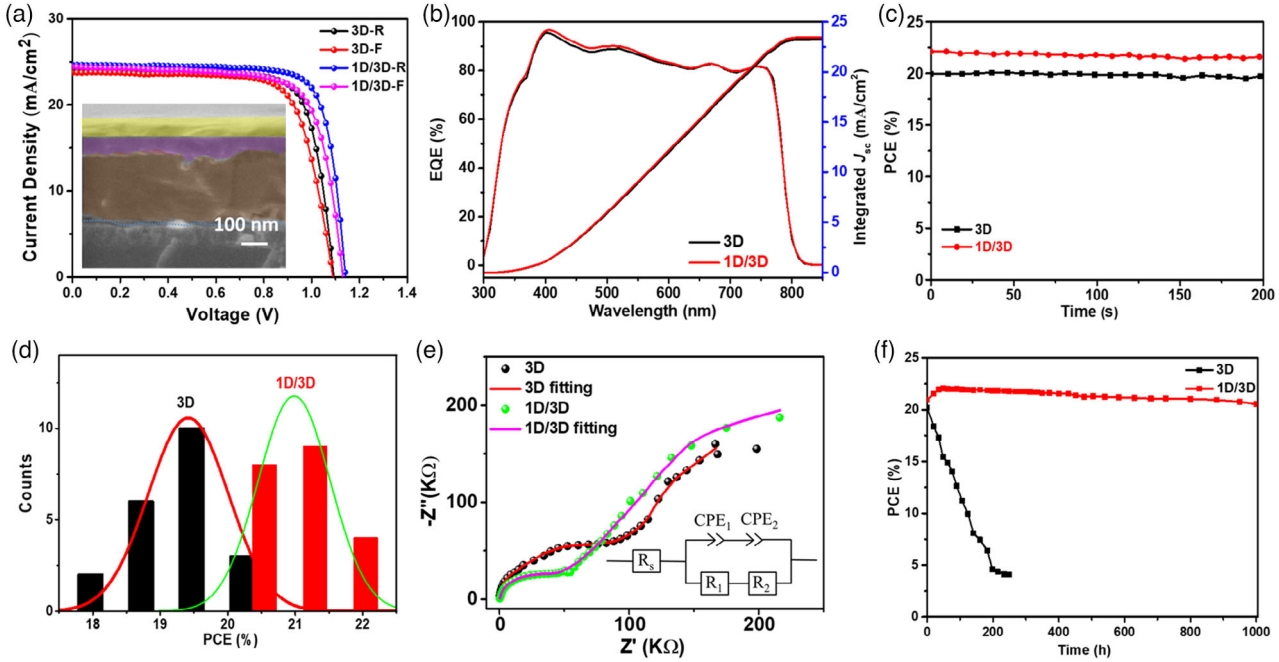

Figure 4. a) *J–V* curve for the photovoltaic performance of a 3D and 1D/3D device; Inset shows the cross-sectional SEM image of the device. b) The corresponding EQE measurement and the integrated J_{sc} of 3D and 1D/3D PSCs; c) The steady-state PCE of the champion 3D and 1D/3D devices; d) Histogram of the PCE for 3D and 1D/3D device; e) Nyquist plots of the 3D and 1D/3D PSCs; inset: equivalent circuit. f) stability tests of unencapsulated 3D and 1D/3D PSCs under ambient conditions (RH ≈ over 50%).

be $1.32 \times 10^{16}\,cm^{-3}$ for the 3D perovskite film and $0.88 \times 10^{16}\,cm^{-3}$ for 1D/3D film, implying that Me_3SI could effectively diminish electron trap density in the perovskite films and thus significantly suppress the trap-assisted nonradiative recombination.

To evaluate photovoltaic performance of the device with and without 1D Me_3SPbI_3 incorporation, we assembled PSCs with the structure of ITO/SnO_2/3D or 1D/3D perovskite/ Spiro-OMeTAD/Au (as shown in inset of **Figure 4**a). When the concentration of Me_3SI was 0.2 mg mL^{-1}, a maximum PCE of 22.07% was obtained while the PCE was 20.10% for the 3D counterpart (Figure 4a), with an enhancement of V_{oc} from 1.09 to 1.14 V, J_{sc} from 24.14 to 24.64 mA cm^{-2}, FF from 76.30% to 78.57%; while the *J–V* cure and the photovoltaic parameters with various adding concentrations of Me_3SI was presented in Figure S4 and Table S3, Supporting Information. Moreover, the champion efficiency is comparable with the published results as shown in Table S4, Supporting Information. Figure 4b displays the external quantum efficiency (EQE) and the integrated current density for the 3D and 1D/3D perovskite based devices. Meanwhile, the corresponding integrated photocurrent density (23.24 and 23.56 mA cm^{-2}) from the measured EQE spectra is consistent with the measured short-circuit current J_{sc} value, the discrepancy is less than by 5%.[20] Figure 4c displays the tracking of the maximum power point (MPP) for 3D and 1D/3D perovskite-based devices over 200 s. The stabilized power output (SPO) efficiency of 19.83% and 21.65% are obtained, in agreement with the *J–V* measurement, suggesting good stability of 1D/3D perovskite-based devices. The histogram of two batches of cells displays the good reproducibility and also verifies the PCE enhancement (Figure 4d). To further study the charge transfer kinetics of the 3D and 1D/3D perovskite-based devices, the electrochemical impedance spectroscopy (EIS) was performed in the frequency range from 0.1 Hz to 1 MHz under dark condition (Figure 4e). The featured semicircle at low frequency (second one) and high frequency (first one) could be assigned to the recombination resistance (R_2) in the devices and the charge transport resistance (R_1) at the interfaces between the carrier (electron or hole) selective layer and the perovskite light absorption layer, respectively.[56] Compared to the 3D device, the 1D/3D device present larger R_2 and lower R_1, suggesting higher charge transfer rate and lower recombination rate and resulting in higher device performance, which can also explain the higher V_{oc} of 1D/3D device.[57] Moreover, we also monitored the long-term stability for the un-encapsulated devices under different conditions. As shown in Figure 4f, the devices with 0.2 mg mL^{-1} Me_3SI addition can maintain 97% of their initial value of PCE after 1000 h storage under ambient with 50% RH.

3. Conclusion

In summary, we have synthesized a sulfur-based 1D perovskite Me_3SPbI_3 in aqueous medium and the PSCs fabricated with this pure 1D Me_3SPbI_3 material exhibited excellent environmental stability with a PCE of 2.08%. By applying this 1D Me_3SPbI_3 into traditional 3D perovskite material, we successfully fabricated 1D/3D heterostructure perovskite layer with remarkably improved stability. The 1D Me_3SPbI_3 perovskite has passivated 3D perovskite surface. The champion device shows a PCE of 22.06%. Importantly, it can maintain 97 % its initial PCE after storage under ambient condition with 50% RH for over 1000 h.

Supporting Information

Supporting Information is available from the Wiley Online Library or from the author.

Acknowledgements

The financial support from the National Natural Science Foundation of China (62004129; 22005202), Shenzhen Science and Technology Innovation Commission (project no. JCYJ20200109105003940) is gratefully acknowledged and this study is supported by Post-Doctoral Foundation Project of Shenzhen Polytechnic 6021330007K.

Conflict of Interest

The authors declare no conflict of interest.

Data Availability Statement

The data that support the findings of this study are available from the corresponding author upon reasonable request.

Keywords

aqueous synthesis, perovskite solar cells, stability, trimethylsulfonium lead triiodide 1D/3D heterostructures

Received: October 21, 2021
Revised: December 10, 2021
Published online:

[1] J. Y. Kim, J.-W. Lee, H. S. Jung, H. Shin, N.-G. Park, *Chem. Rev.* **2020**, *120*, 7867.
[2] H. Hu, M. Singh, X. Wan, J. Tang, C.-W. Chu, G. Li, *J. Mater. Chem. A* **2020**, *8*, 1578.
[3] C. Ge, Y. Z. Xue, L. Li, B. Tang, H. Hu, *Front. Mater.* **2020**, *7*, https://doi.org/10.3389/fmats.2020.601179.
[4] C. Yang, R. Zhi, M. U. Rothmann, F. Huang, Y.-B. Cheng, W. Li, *Sol. RRL* **2021**, 2100600.
[5] L. Chu, L. Ding, *J. Semicond.* **2021**, *42*, 090202.
[6] A. Kojima, K. Teshima, Y. Shirai, T. Miyasaka, *J. Am. Chem. Soc.* **2009**, *131*, 6050.
[7] J. Jeong, M. Kim, J. Seo, H. Lu, P. Ahlawat, A. Mishra, Y. Yang, M. A. Hope, F. T. Eickemeyer, M. Kim, Y. J. Yoon, I. W. Choi, B. P. Darwich, S. J. Choi, Y. Jo, J. H. Lee, B. Walker, S. M. Zakeeruddin, L. Emsley, U. Rothlisberger, A. Hagfeldt, D. S. Kim, M. Gratzel, J. Y. Kim, *Nature* **2021**, *592*, 381.
[8] H. Min, D. Y. Lee, J. Kim, G. Kim, K. S. Lee, J. Kim, M. J. Paik, Y. K. Kim, K. S. Kim, M. G. Kim, T. J. Shin, S. Il Seok, *Nature* **2021**, *598*, 444.
[9] T. Kong, H. Xie, Y. Zhang, J. Song, Y. Li, E. L. Lim, A. Hagfeldt, D. Bi, *Adv. Energy Mater.* **2021**, *11*, 2101018.
[10] D. Wang, M. Wright, N. K. Elumalai, A. Uddin, *Sol. Energy Mater. Sol. Cells* **2016**, *147*, 255.
[11] M. V. Khenkin, E. A. Katz, A. Abate, G. Bardizza, J. J. Berry, C. Brabec, F. Brunetti, V. Bulović, Q. Burlingame, A. Di Carlo, R. Cheacharoen, Y.-B. Cheng, A. Colsmann, S. Cros, K. Domanski, M. Dusza, C. J. Fell, S. R. Forrest, Y. Galagan, D. Di Girolamo, M. Grätzel, A. Hagfeldt, E. von Hauff, H. Hoppe, J. Kettle, H. Köbler, M. S. Leite, S. Liu, Y.-L. Loo, J. M. Luther, et al., *Nat. Energy* **2020**, *5*, 35.
[12] Z. Yang, B. H. Babu, S. Wu, T. Liu, S. Fang, Z. Xiong, L. Han, W. Chen, *Sol. RRL* **2020**, *4*, 1900257.
[13] L. Chu, *Matter* **2021**, *4*, 1762.
[14] C. Ma, D. Shen, B. Huang, X. Li, W. C. Chen, M. F. Lo, P. Wang, M. Hon-Wah Lam, Y. Lu, B. Ma, C. S. Lee, *J. Mater. Chem. A* **2019**, *7*, 8811.
[15] H. Lin, C. Zhou, Y. Tian, T. Siegrist, B. Ma, *ACS Energy Lett.* **2018**, *3*, 54.
[16] D.-K. Lee, N.-G. Park, *Sol. RRL* **2021**, 2100455.
[17] Q. A. Akkerman, S. G. Motti, A. R. Srimath Kandada, E. Mosconi, V. D'Innocenzo, G. Bertoni, S. Marras, B. A. Kamino, L. Miranda, F. De Angelis, A. Petrozza, M. Prato, L. Manna, *J. Am. Chem. Soc.* **2016**, *138*, 1010.
[18] J. V. Milić, J. Im, D. J. Kubicki, A. Ummadisingu, J. Seo, Y. Li, M. A. Ruiz-Preciado, M. I. Dar, S. M. Zakeeruddin, L. Emsley, M. Grätzel, *Adv. Energy Mater.* **2019**, *9*, 1900284.
[19] C. Zhou, Y. Tian, M. Wang, A. Rose, T. Besara, N. K. Doyle, Z. Yuan, J. C. Wang, R. Clark, Y. Hu, T. Siegrist, S. Lin, B. Ma, *Angew. Chem., Int. Ed.* **2017**, *56*, 9018.
[20] P. Liu, Y. Xian, W. Yuan, Y. Long, K. Liu, N. U. Rahman, W. Li, J. Fan, *Adv. Energy Mater.* **2020**, *10*, 1903654.
[21] A. Kaltzoglou, M. M. Elsenety, I. Koutselas, A. G. Kontos, K. Papadopoulos, V. Psycharis, C. P. A. Kaltzoglou, G. K. Manolis, M. M. Elsenety, I. Koutselas, V. Psycharis, A. G. Kontos, P. Falaras, *J. Electron. Mater.* **2019**, *48*, 7533.
[22] C. C. Stoumpos, L. Mao, C. D. Malliakas, M. G. Kanatzidis, *Inorg. Chem.* **2017**, *56*, 56.
[23] R. Kaneko, H. Kanda, N. Shibayama, K. Sugawa, J. Otsuki, A. Islam, M. K. Nazeeruddin, *Sol. RRL* **2021**, *5*, 4.
[24] M. S. de Holanda, R. Szostak, P. E. Marchezi, L. G. T. A. Duarte, J. C. Germino, T. D. Z. Atvars, A. F. Nogueira, *Sol. RRL* **2019**, *3*, 1900199.
[25] G. Liu, H. Zheng, J. Ye, S. Xu, L. Zhang, H. Xu, Z. Liang, X. Chen, X. Pan, *ACS Energy Lett.* **2021**, *6*, 4395.
[26] D. Bi, P. Gao, R. Scopelliti, E. Oveisi, J. Luo, M. Grätzel, A. Hagfeldt, M. K. Nazeeruddin, *Adv. Mater.* **2016**, *28*, 2910.
[27] J. Fan, Y. Ma, C. Zhang, C. Liu, W. Li, R. E. I. Schropp, Y. Mai, *Adv. Energy Mater.* **2018**, *8*, 1703421.
[28] S. Yu, H. Liu, S. Wang, H. Zhu, X. Dong, X. Li, *Chem. Eng. J.* **2021**, *403*, 125724.
[29] L. Gao, I. Spanopoulos, W. Ke, S. Huang, I. Hadar, L. Chen, X. Li, G. Yang, M. G. Kanatzidis, *ACS Energy Lett.* **2019**, *4*, 1763.
[30] A. F. Xu, N. Liu, F. Xie, T. Song, Y. Ma, P. Zhang, Y. Bai, Y. Li, Q. Chen, G. Xu, *Nano Lett.* **2020**, *20*, 3864.
[31] N. Yang, C. Zhu, Y. Chen, H. Zai, C. Wang, X. Wang, H. Wang, S. Ma, Z. Gao, X. Wang, J. Hong, Y. Bai, H. Zhou, B. Bin Cui, Q. Chen, *Energy Environ. Sci.* **2020**, *13*, 4344.
[32] M. M. Rahman, A. Ahmed, C. Ge, R. Singh, K. Yoo, S. Sandhu, S. Kim, J.-J. Lee, *Sustainable Energy Fuels* **2021**, *5*, 4327.
[33] A. Kaltzoglou, M. M. Elsenety, I. Koutselas, A. G. Kontos, K. Papadopoulos, V. Psycharis, C. P. Raptopoulou, D. Perganti, T. Stergiopoulos, P. Falaras, *Polyhedron* **2018**, *140*, 67.
[34] A. Kaltzoglou, C. C. Stoumpos, A. G. Kontos, G. K. Manolis, K. Papadopoulos, K. G. Papadokostaki, V. Psycharis, C. C. Tang, Y.-K. Jung, A. Walsh, M. G. Kanatzidis, P. Falaras, *Inorg. Chem.* **2017**, *56*, 6302.
[35] M. M. Elsenety, A. Kaltzoglou, M. Antoniadou, I. Koutselas, A. G. Kontos, P. Falaras, *Polyhedron* **2018**, *150*, 83.
[36] M. M. Elsenety, M. Antoniadou, A. Kaltzoglou, A. G. Kontos, A. I. Philippopoulos, C. A. Mitsopoulou, P. Falaras, *Mater. Chem. Phys.* **2020**, *239*, 122310.

[37] R. Hu, C. Ge, L. Chu, Y. Feng, S. Xiao, Y. Ma, W. Liu, X. Li, M. K. Nazeeruddin, *J. Energy Chem.* **2021**, *59*, 581.
[38] Y. Wu, A. Islam, X. Yang, C. Qin, J. Liu, K. Zhang, W. Peng, L. Han, *Energy Environ. Sci.* **2014**, *7*, 2934.
[39] Y. Zhang, Z. Zhou, F. Ji, Z. Li, G. Cui, P. Gao, E. Oveisi, M. K. Nazeeruddin, S. Pang, *Adv. Mater.* **2018**, *30*, 1707143.
[40] S. Rühle, *Sol. Energy* **2016**, *130*, 139.
[41] Y. Han, S. Yue, B. Cui, *Adv. Sci.* **2021**, *8*, 2004805.
[42] B. Zhao, S. Bai, V. Kim, R. Lamboll, R. Shivanna, F. Auras, J. M. Richter, L. Yang, L. Dai, M. Alsari, X.-J. She, L. Liang, J. Zhang, S. Lilliu, P. Gao, H. J. Snaith, J. Wang, N. C. Greenham, R. H. Friend, D. Di, *Nat. Photonics* **2018**, *12*, 783.
[43] E. A. Alharbi, A. Y. Alyamani, D. J. Kubicki, A. R. Uhl, B. J. Walder, A. Q. Alanazi, J. Luo, A. Burgos-Caminal, A. Albadri, H. Albrithen, M. H. Alotaibi, J.-E. Moser, S. M. Zakeeruddin, F. Giordano, L. Emsley, M. Grätzel, *Nat. Commun.* **2019**, *10*, 3008.
[44] M. Parashar, R. Singh, K. Yoo, J. J. Lee, *ACS Appl. Energy Mater.* **2021**, *4*, 2751.
[45] Z. Yuan, C. Zhou, Y. Tian, Y. Shu, J. Messier, J. C. Wang, L. J. van de Burgt, K. Kountouriotis, Y. Xin, E. Holt, K. Schanze, R. Clark, T. Siegrist, B. Ma, *Nat. Commun.* **2017**, *8*, 14051.
[46] M. Qin, H. Xue, H. Zhang, H. Hu, K. Liu, Y. Li, Z. Qin, J. Ma, H. Zhu, K. Yan, G. Fang, G. Li, U. Jeng, G. Brocks, S. Tao, X. Lu, *Adv. Mater.* **2020**, *32*, 2004630.
[47] Q. Jiang, Y. Zhao, X. Zhang, X. Yang, Y. Chen, Z. Chu, Q. Ye, X. Li, Z. Yin, J. You, *Nat. Photonics* **2019**, *13*, 460.
[48] L. Zuo, H. Guo, D. W. DeQuilettes, S. Jariwala, N. De Marco, S. Dong, R. DeBlock, D. S. Ginger, B. Dunn, M. Wang, Y. Yang, *Sci. Adv.* **2017**, *3*, e1700106.
[49] Q. Chen, H. Zhou, T.-B. Song, S. Luo, Z. Hong, H.-S. Duan, L. Dou, Y. Liu, Y. Yang, *Nano Lett.* **2014**, *14*, 4158.
[50] Y. Guo, W. Sato, K. Shoyama, H. Halim, Y. Itabashi, R. Shang, E. Nakamura, *J. Am. Chem. Soc.* **2017**, *139*, 9598.
[51] T. Kong, H. Xie, Y. Zhang, J. Song, Y. Li, E. L. Lim, A. Hagfeldt, D. Bi, *Adv. Energy Mater.* **2021**, *11*, 2101018.
[52] Z. He, Y. Zhou, C. Xu, Y. Su, A. Liu, Y. Li, L. Gao, T. Ma, *J. Phys. Chem. C* **2021**, *125*, 16428.
[53] H. Cho, S.-H. Jeong, M.-H. Park, Y.-H. Kim, C. Wolf, C.-L. Lee, J. H. Heo, A. Sadhanala, N. Myoung, S. Yoo, S. H. Im, R. H. Friend, T.-W. Lee, *Science* **2015**, *350*, 1222.
[54] V. Adinolfi, M. Yuan, R. Comin, E. S. Thibau, D. Shi, M. I. Saidaminov, P. Kanjanaboos, D. Kopilovic, S. Hoogland, Z.-H. Lu, O. M. Bakr, E. H. Sargent, *Adv. Mater.* **2016**, *28*, 3406.
[55] Y. Huang, L. Li, Z. Liu, H. Jiao, Y. He, X. Wang, R. Zhu, D. Wang, J. Sun, Q. Chen, H. Zhou, *J. Mater. Chem. A* **2017**, *5*, 8537.
[56] H. Zhang, J. Mao, H. He, D. Zhang, H. L. Zhu, F. Xie, K. S. Wong, M. Grätzel, W. C. H. Choy, *Adv. Energy Mater.* **2015**, *5*, 1501354.
[57] X. Jiang, J. Zhang, S. Ahmad, D. Tu, X. Liu, G. Jia, X. Guo, C. Li, *Nano Energy* **2020**, *75*, 104892.